Rapid and accurate large-scale genotyping of duplicated genes and discovery of interlocus gene conversions

Xander Nuttle[1], John Huddleston[1,2], Brian J O'Roak[1], Francesca Antonacci[1,6], Marco Fichera[3,4], Corrado Romano[5], Jay Shendure[1] & Evan E Eichler[1,2]

Over 900 genes have been annotated within duplicated regions of the human genome, yet their functions and potential roles in disease remain largely unknown. One major obstacle has been the inability to accurately and comprehensively assay genetic variation for these genes in a high-throughput manner. We developed a sequencing-based method for rapid and high-throughput genotyping of duplicated genes using molecular inversion probes designed to target unique paralogous sequence variants. We applied this method to genotype all members of two gene families, *SRGAP2* and *RH*, among a diversity panel of 1,056 humans. The approach could accurately distinguish copy number in paralogs having up to ~99.6% sequence identity, identify small gene-disruptive deletions, detect single-nucleotide variants, define breakpoints of unequal crossover and discover regions of interlocus gene conversion. The ability to rapidly and accurately genotype multiple gene families in thousands of individuals at low cost enables the development of genome-wide gene conversion maps and 'unlocks' many previously inaccessible duplicated genes for association with human traits.

Duplicated genes are important contributors to genetic variation[1–4], evolutionary adaptation[5–8] and human disease[9–12]. Despite this, most individual duplicated genes remain poorly characterized at the genetic level[13] because of high sequence identity[13,14], extensive copy-number polymorphism[1–4], missing sequencing data[13] and low correlation with flanking single-nucleotide polymorphisms[2,15,16]. As a result, these genes and regions have often been excluded from genetic analyses[17,18], or contradictory associations with disease have been reported[19,20].

Several different technologies have been applied to assay copy number for such genes[21]. Both quantitative real-time PCR (qPCR) and the paralog ratio test[22], which uses PCR product specificity to distinguish copies, are labor intensive, requiring the design and testing of multiple primers. Multiplex ligation-dependent probe amplification (MLPA)[23] and multiplex amplification and probe hybridization (MAPH)[24] allow for copy-number analysis at up to 50 loci simultaneously, but they cannot be applied to genotype many gene families at high spatial resolution in a single reaction. Array comparative genomic hybridization (CGH) lacks paralog specificity and can access only a fraction of duplicated genes, typically where the number of duplicated copies is low[2,16]. Finally, mapping whole-genome sequencing (WGS) data to singly unique nucleotide (SUN) identifiers that tag a particular paralog and analyzing the read depth[1,25] has yielded genome-wide paralog-specific copy-number estimates. However, the sensitivity of this approach depends on genome sequencing coverage, and sequencing remains a costly proposition that cannot be applied to thousands of samples in a laboratory setting.

Here we used molecular inversion probes (MIPs), short oligonucleotides designed to capture targeted genomic regions[26–29], together with massively parallel DNA sequencing for genotyping duplicated genes. We evaluated this method by examining *SRGAP2* and *RH* genetic variation in 1,056 individuals and explored its potential application to the discovery of interlocus gene-conversion events in humans. The method scaled well to thousands of samples and yielded accurate, paralog-specific sequence and copy-number genotypes at a low cost.

RESULTS

Genotyping strategy

Our approach leverages SUN variants, fixed paralogous sequence variants that uniquely tag a specific paralog and distinguish it from all other copies[1]. We systematically designed MIPs to hybridize to sequences that are identical between paralogs flanking SUNs across the length of the duplicated segment (**Fig. 1**, **i**,**ii** and Online Methods) and additional MIP assays targeting exons in the paralogs to assay coding-sequence variation. The probability of an individual MIP capturing sequence from a particular paralog is a function of its copy number relative to the copy number of related paralogs (**Fig. 1**, **iii**). Massively parallel sequencing of amplified capture products allows simultaneous quantification of sequences derived from each paralog (**Fig. 1**, **iv**) and detection of sequence-level genetic variation. We selected two gene families to

[1]Department of Genome Sciences, University of Washington School of Medicine, Seattle, Washington, USA. [2]Howard Hughes Medical Institute, University of Washington School of Medicine, Seattle, Washington, USA. [3]Regional Center for Genetic Rare Diseases with Intellectual Disability or Brain Aging, Fondazione Santa Lucia Istituto di Ricovero e Cura a Carattere Scientifico (IRCCS), Troina, Italy. [4]Medical Genetics, University of Catania, Catania, Italy. [5]Pediatrics and Medical Genetics, Istituto di Ricovero e Cura a Carattere Scientifico (IRCCS) Associazione Oasi Maria Santissima, Troina, Italy. [6]Present address: Department of Biology, University of Bari, Bari, Italy. Correspondence should be addressed to E.E.E. (eee@gs.washington.edu).

RECEIVED 4 MARCH; ACCEPTED 6 JUNE; PUBLISHED ONLINE 28 JULY 2013; CORRECTED ONLINE 13 AUGUST 2013 (DETAILS ONLINE); DOI:10.1038/NMETH.2572

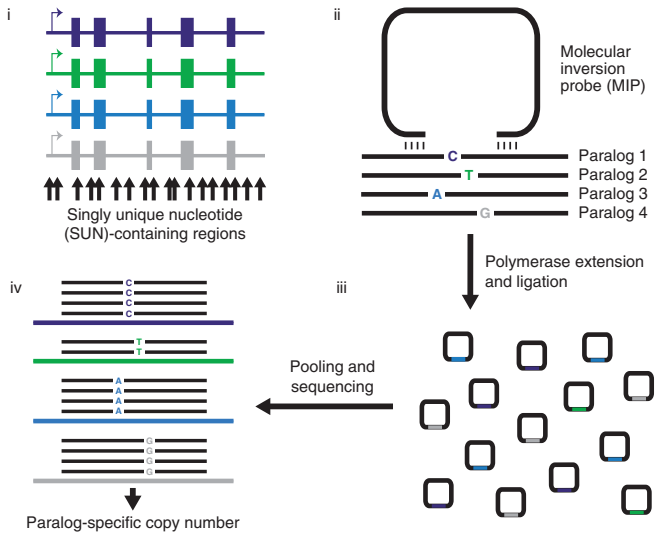

Figure 1 | MIP copy-number genotyping assay for duplicated genes. (**i**) 112-nucleotide (nt) regions (black arrows) containing sequence variants that uniquely distinguish one paralog (potential SUNs) are identified through alignment of genomic sequence. (**ii**) 70-nt MIPs used for copy-number genotyping have 16- to 24-nt hybridization arms complementary to sequence flanking SUN-containing regions. Several such MIPs are designed, collectively spanning the spatial extent of duplicated genic sequence. (**iii**) DNA polymerase extension and ligation incorporates SUN-containing sequences into covalently closed circular molecules, which are then barcoded, pooled and sequenced. (**iv**) Reads are mapped to reference sequences for each paralog, and paralog-specific read counts for each MIP are quantified. A genotyping program infers paralog-specific copy number from these counts. The schematic shows counts consistent with a deletion of paralog 2 (green).

demonstrate the proof of principle of our approach and to assess its power to discover novel genetic variation in duplicated regions: *SRGAP2* (ref. 13), a highly identical (>99%) human-specific gene family, and *RH*, a clinically relevant blood-antigen gene family that has been extensively characterized for common copy-number polymorphism[30], rearrangement breakpoints[31] and interlocus gene conversion[32] in the human population.

Copy-number and sequence genotyping

For *SRGAP2*, we designed a total of 142 MIPs targeted to sites corresponding to potential SUNs (**Supplementary Tables 1** and **2** and Online Methods) that could reliably differentiate *SRGAP2* paralogs. Forty of these MIP targets harbor nucleotide differences that distinguish all four *SRGAP2* paralogs from one another, 28 distinguish two *SRGAP2* paralogs from the other two paralogs, and the remaining 74 distinguish a single *SRGAP2* paralog from the remaining three. We initially used these MIPs to genotype 48 individuals for which orthogonal *SRGAP2* copy-number data were generated or were available from WGS data (Online Methods), array CGH and/or FISH. All captured sequences from a given DNA sample were barcoded, pooled with those from other samples and sequenced using HiSeq or MiSeq (Illumina) to an approximate coverage of 350 reads per MIP per individual. For each individual, paralog-specific read counts served as a proxy for copy number for each *SRGAP2* gene. We developed a maximum-likelihood approach using paralog-specific read-count data to generate *SRGAP2* paralog-specific copy-number calls across the spatial extent of duplicated *SRGAP2* sequence (Online Methods). Incorporating data from all MIPs overwhelms noisy signals from poorly performing individual MIPs. Plotting MIP data for 90 high-performing copy-number MIPs (Online Methods and **Supplementary Figs. 1** and **2**) alongside FISH data for three representative individuals highlights the precision with which MIP genotyping detected known duplications and deletions of *SRGAP2B* and *SRGAP2D* (**Fig. 2**).

We found that 97.2% (35 of 36) of copy-number calls were concordant with FISH, 8 of 8 were consistent with array CGH data, and 91.5% (150 of 164) agreed with estimates made from WGS data (**Supplementary Table 3**). All inconsistencies involved genotyping results for the *SRGAP2D* pseudogene. This paralog is the shortest and most recently duplicated segment having ~99.6% identity to *SRGAP2B*. Low WGS coverage together with the paucity of *SRGAP2D* SUNs likely confounded sequencing-based copy-number estimates for *SRGAP2D*. To explore this possibility, we generated aggregate *SRGAP2* copy-number estimates from WGS data. These aggregate estimates are more accurate than corresponding paralog-specific estimates[1] because all reads mapping to *SRGAP2* (rather than just those mapping to SUN identifiers) inform this analysis. Notably, 13 of 14 aggregate *SRGAP2* copy-number estimates were consistent with MIP-based paralog-specific estimates rather than with corresponding WGS-based paralog-specific estimates in cases when these results disagreed. We extended our analysis to include 1,056 HapMap individuals, 73 of which we genotyped more than once using MIPs to examine the reproducibility of our approach. We found 99.5% (390 of 392) of replicate *SRGAP2* paralog-specific copy-number genotypes were concordant with initial MIP-based genotypes (**Supplementary Table 4**).

Our data allowed us to estimate allele frequencies for *SRGAP2* duplications and deletions in nine human populations (**Supplementary Table 5**). As expected from a previous analysis of WGS data[13], *SRGAP2B* and *SRGAP2D* showed evidence of complete loss or gain, ranging in copy number from 0 to 4 in the human population. In contrast, complete duplication or deletion of *SRGAP2A* or *SRGAP2C* was not observed, a result consistent with the notion that these two paralogs are functional copies. Our analysis of *SRGAP2B* and *SRGAP2D* copy-number variation suggests population stratification. Deletion of *SRGAP2B*, for example, is more common in populations of African descent than deletions of *SRGAP2D*, which segregate at higher frequencies in several out-of-Africa populations.

Unlike most other copy-number genotyping assays, MIPs also provide information on the sequence content of targeted regions[28,29,33]. We reasoned that in some cases, linkage of discovered single-nucleotide variants (SNVs) to a nearby paralog-distinguishing SUN would allow inference of the paralog of origin. We evaluated whether our method could accurately genotype such SNVs by comparing MIP sequence data (Online Methods) with fosmid clone end-sequence data[34] and WGS data for NA18507, an individual previously sequenced to high coverage[35]. The WGS data validated 93.8% (15 of 16) of our genotype calls (**Supplementary Table 6**), including a heterozygous nonsynonymous variant. Fosmid end-sequence data including a putative variant site were available in only three cases, but each validated the SNV identified from MIP data. Thus, our method can successfully

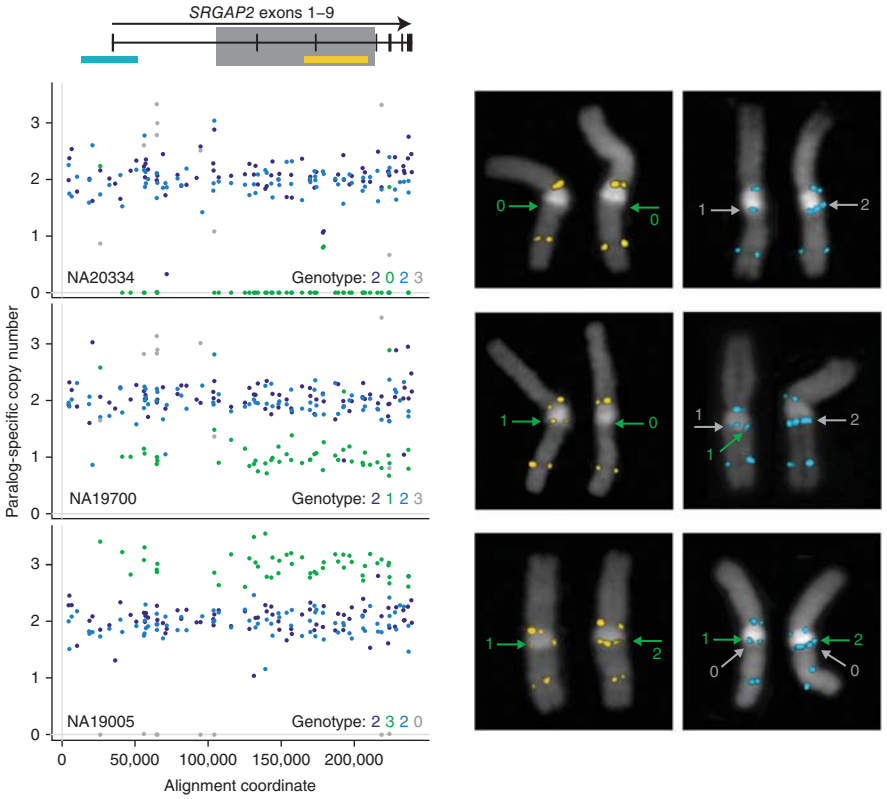

Figure 2 | Accuracy of paralog-specific copy-number genotyping. MIPs (142) and FISH were used for genotyping *SRGAP2* copy number in the HapMap individuals NA20334, NA19700 and NA19005. Exon locations are plotted relative to the FISH probes (cyan and yellow rectangles) and MIP data below. The gray box indicates the region deleted in *SRGAP2D*. Paralog-specific copy-number estimates are shown for 90 high-performing MIPs across ~240 kbp of aligned *SRGAP2* genomic sequence. Each point indicates a paralog-specific copy-number estimate (purple, *SRGAP2A*; green, *SRGAP2B*; blue, *SRGAP2C*; gray, *SRGAP2D*), calculated as the product of the paralog-specific read-count frequency for a particular MIP and the aggregate estimated *SRGAP2* copy number at the corresponding locus. Shown are homozygous and heterozygous deletions and a duplication of *SRGAP2B* as well as duplications and a homozygous deletion of *SRGAP2D*. Right, FISH data validate the MIP-based paralog-specific copy-number genotypes for these individuals. Colored numbers indicate copy number of *SRGAP2B* or *SRGAP2D* for the adjacent chromosome. FISH data for NA20334 and NA19700 are consistent with either two or three diploid copies of the *SRGAP2D* paralog.

detect SNVs within highly identical duplicated sequence and in some cases accurately assign them to specific paralogs.

Internal *SRGAP2* deletion and duplication discovery

We applied our MIP-based method to two individuals having array CGH profiles showing complex structural variation in *SRGAP2* (ref. 13). MIP genotyping correctly identified large *SRGAP2C* and *SRGAP2A* events discovered via array CGH and resolved the internal deletions as specifically affecting *SRGAP2C*, removing exon 2 and inducing a frameshift (**Fig. 3**). MIP-based genotyping of 1,056 HapMap individuals indicated that this deletion is segregating at low frequency (<3%) exclusively in populations with some European ancestry. In addition to this *SRGAP2C* deletion, we identified seven other additional internal deletion and duplication events in HapMap individuals ranging in size from 1.5 kilobase pairs (kbp) to 144 kbp and assigned them to specific *SRGAP2* paralogs (**Supplementary Table 5** and **Supplementary Fig. 3**). These structural variants included three distinct exon-overlapping events in *SRGAP2B* and an intronic duplication in *SRGAP2A*.

RH gene conversion, copy number and breakpoint resolution

To assess the applicability of our method to assaying interlocus gene conversion and resolving breakpoints associated with nonallelic homologous recombination (NAHR), we applied our MIP genotyping method to *RHD* and *RHCE*—sites of known gene conversion and unequal crossover with clinical relevance for Rh antigen presentation. We reasoned that these two forms of mutation would generate characteristic sequence signatures with respect to SUN copy number. In the case of gene conversion, we would expect to observe a reciprocal copy-number shift at a pocket of homology with no difference in copy number of flanking regions. Gains would correspond to donors and losses to acceptors of gene conversion, allowing inference of the directionality of the event. In contrast, at a site of unequal crossover,

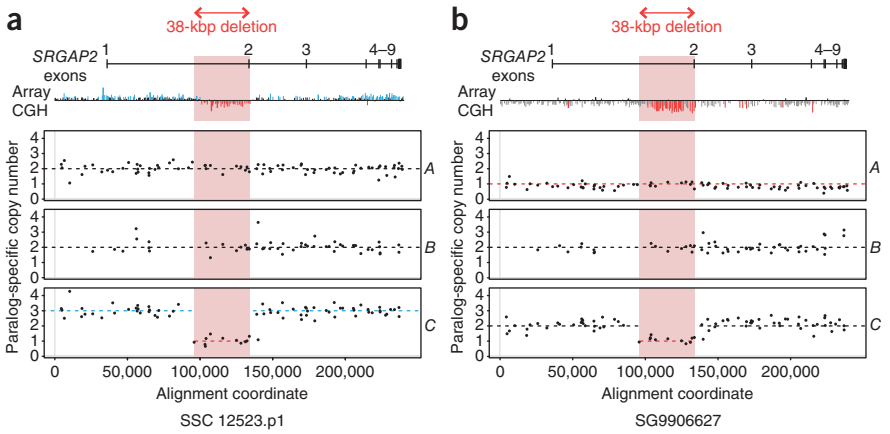

Figure 3 | Resolution of complex structural variation in *SRGAP2*. (**a**) The array CGH profile for *SRGAP2* loci predicts a gain and an interstitial loss for a patient with autism but cannot distinguish which paralogs the variation affects. The MIP copy-number assay predicts two copies for *A*, *B* and *D* (not shown) but duplication of a copy of *C* having an ~38-kbp internal deletion containing exon 2. Dashed lines indicate paralog-specific copy-number calls from the automated caller. (**b**) Similar analysis of a patient with developmental delay shows that the individual is diploid for *B* and *D* (not shown) but has lost a copy of *A* (the ancestral locus) and carries the internal deletion for *C*.

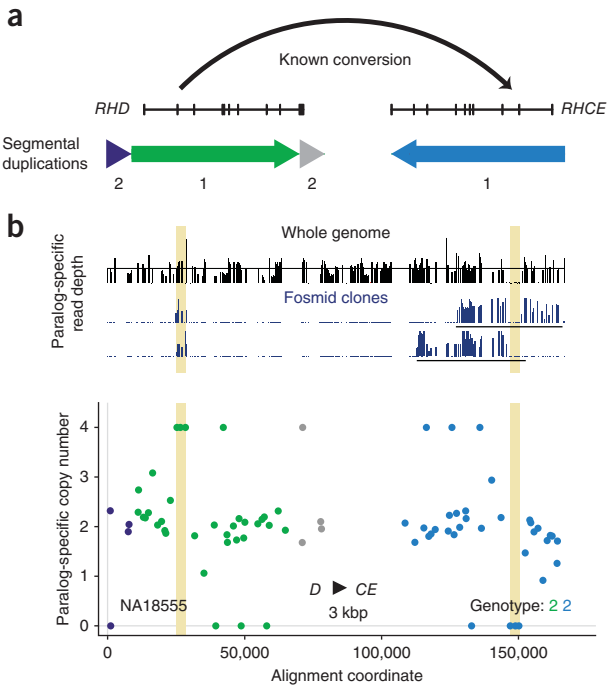

Figure 4 | Detection of gene conversion at the *RH* locus. (**a**) *RHD* and *RHCE* lie within an ~60-kbp segmental duplication (green and blue arrows) and frequently undergo interlocus gene-conversion events. (**b**) MIPs (39) were used for genotyping paralog-specific *RH* copy number in the HapMap individual NA18555. MIP data (bottom) are plotted relative to locations of *RH* exons and associated segmental duplications in **a**. Colors correspond to segmental duplications shown in **a**. A homozygous gene conversion from *RHD* to *RHCE* spanning at least ~3 kbp at a known conversion site including exon 2 is highlighted in yellow. We validated this homozygous conversion by mapping whole-genome and fosmid clone short-read sequence data from this individual to SUN identifiers and examining paralog-specific read depth.

a reciprocal SUN copy-number transition should be observed around the NAHR breakpoint.

We designed 39 MIPs targeting *RH* paralogs and flanking regions (**Fig. 4a**) and included them in the same capture reactions as *SRGAP2* MIPs, which allowed us to simultaneously genotype the same individuals described above for *RH*. Searching for reciprocal copy-number shifts, we observed seven distinct putative *RH* gene-conversion events, ranging in length from 1,709 base pairs (bp) to ~39 kbp (**Supplementary Table 5** and **Supplementary Fig. 4**). Although we denote these events as gene conversions, other mutational mechanisms[36–38] may be responsible for the signatures we observed. Four events involved a transfer of genetic information from *RHCE* to *RHD*, four corresponded to polymorphic variants reported in the Blood Group Antigen Gene Mutation Database (dbRBC at the US National Center for Biotechnology Information), and four were supported by at least one observed instance of transmission from parent to child. The most common involved sequence transfer from *RHD* to *RHCE* at a known gene-conversion site including *RHD* exon 2 (ref. 39) and was confirmed by whole-genome and fosmid clone sequencing data[1] from an individual predicted from MIP data to be homozygous for this event (**Fig. 4b**).

Using our copy-number genotyping strategy, we identified known deletions and duplications in *RHD* associated with unequal crossover between flanking segmental duplications (**Fig. 5a**).

We found 97.6% (80 of 82) of our *RH* paralog-specific copy-number estimates agreed with those from WGS data (**Supplementary Table 3**). Reproducibility was lower for *RH* copy-number genotyping than for *SRGAP2* genotyping (**Supplementary Table 4**), as only 91.8% (180 of 196) of replicate MIP-based *RH* paralog-specific copy-number genotypes were concordant with initial genotypes. We calculated logarithm-of-odds confidence scores for each of these genotypes (Online Methods) and observed that discordancies' scores fell at the low end of the score distribution (**Supplementary Table 7** and **Supplementary Fig. 5**), a result suggesting that potential errors can be readily distinguished from high-confidence genotype calls. To attempt to refine NAHR-associated breakpoints, we looked for instances of a reciprocal paralog-specific copy-number transition within the segmental duplications flanking *RHD*. This approach allowed us to narrow breakpoint locations to within ~6-kbp windows (**Fig. 5b**), regions previously found to contain *RHD* deletion breakpoints as determine by Sanger sequencing of spanning PCR products[31].

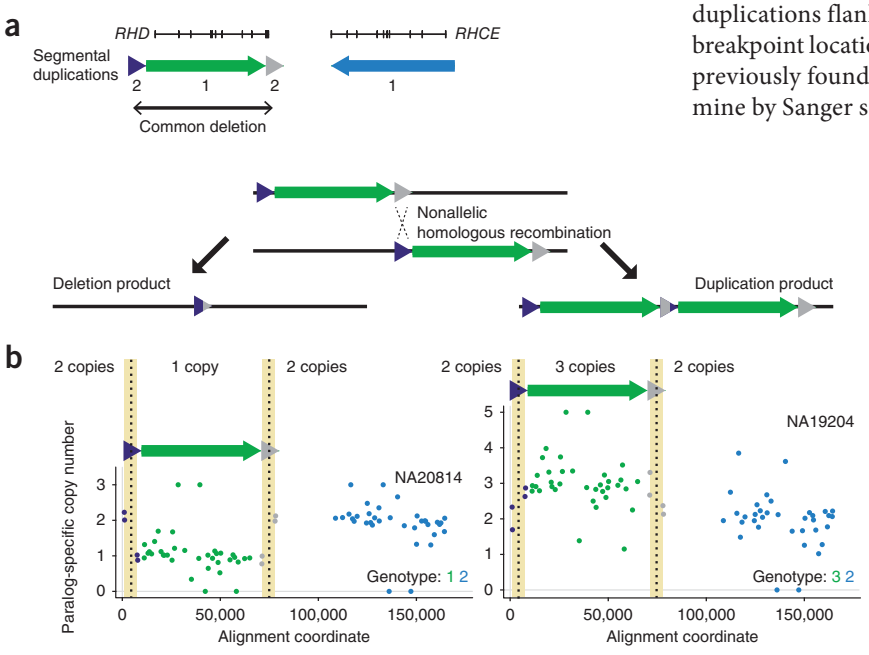

Figure 5 | Resolution of nonallelic homologous recombination (NAHR)-associated *RHD* deletion and duplication breakpoints. (**a**) An ~9-kbp segmental duplication (purple and gray triangles) flanks *RHD*. NAHR between these flanking sequences results in deletion and duplication of *RHD*. (**b**) Data from 39 *RH* MIPs for HapMap individuals NA20814 and NA19204 reveal copy-number variation at *RHD*. Note the signatures of NAHR in the four MIP data points corresponding to the *RHD*-flanking segmental duplications. These data refine the NAHR-associated breakpoints to ~6-kbp homologous genomic regions (highlighted in yellow) where *RHD* deletion breakpoints have been previously reported.

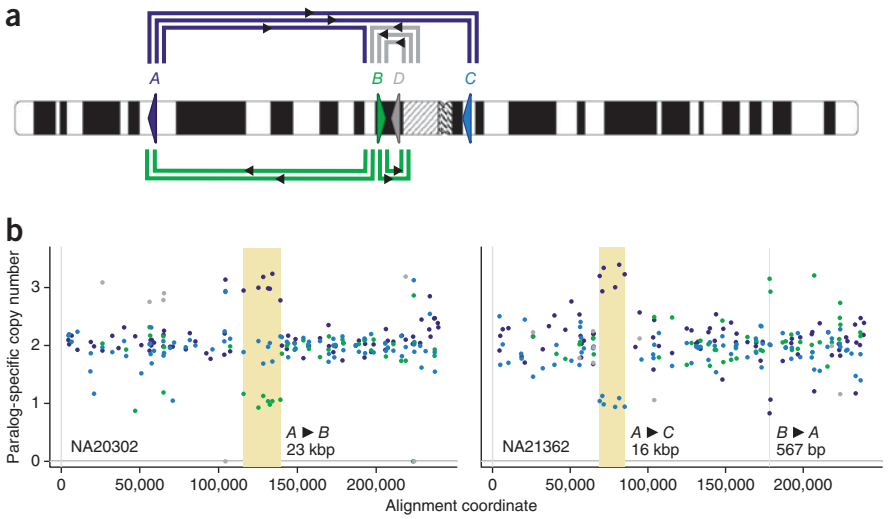

Figure 6 | Extensive interlocus gene conversion between *SRGAP2* paralogs. (**a**) Schematic denoting location and orientation (triangles) of *SRGAP2* paralogs on human chromosome 1. Thick colored lines connect *SRGAP2* paralogs exhibiting signatures of interlocus gene conversion in the MIP data. Line colors correspond to conversion donors, and each line corresponds to a distinct conversion event. (**b**) Examples of different interlocus gene-conversion events (highlighted in yellow). Reported sizes indicate the minimum length of the conversion event based on the MIP data, assuming a single conversion event underlies the conversion signature. All events shown, except for the *B*-to-*A* conversion revealed by two MIPs, were detected by the automated caller.

Discovery of interlocus gene conversions in *SRGAP2*

Given the >99% sequence identity between *SRGAP2* paralogs, we reasoned that interlocus gene conversion or other mechanisms of nonreciprocal sequence transfer may have occurred at these loci and left signatures detectable using our MIP genotyping method. Analysis of the 1,056 HapMap individuals revealed ten such events ranging in size from 416 bp to 23 kbp (**Supplementary Table 5** and **Supplementary Fig. 6**), collectively involving all four *SRGAP2* paralogs (**Fig. 6a**). All paralogs except *SRGAP2C* were observed as putative gene-conversion donors. Unlike *RHD*/*CE*, these putative conversion events appear to have occurred over large genetic distances. For example, two distinct nonreciprocal exchanges of genetic information occur across the centromere between *SRGAP2A* and *SRGAP2C*—paralogs over 80 megabase pairs (Mbp) apart on chromosome 1 (ref. 13; **Fig. 6b** and **Supplementary Fig. 6**).

To corroborate these findings, we examined inheritance for putative gene-conversion events detected in members of HapMap trios. We observed at least one instance of transmission from parent to child for six distinct putative gene conversions, and no such events were inferred as *de novo*. We also validated one putative conversion using paralog-specific qPCR and array CGH. MIP data suggested a complete *SRGAP2D* duplication and a gene conversion resulting in replacement of *SRGAP2C* sequence with paralogous sequence in a patient with intellectual disability (**Supplementary Fig. 7**). If the MIP genotyping were accurate, results from *SRGAP2C*-specific qPCR using primers in the putative conversion region would be expected to signal a loss in *SRGAP2C* copy number, but results from array CGH would be expected to signal a slight gain in aggregate *SRGAP2* copy number over *SRGAP2* sequence shared with *SRGAP2D*. Performing the qPCR and array CGH experiments yielded precisely these results, providing additional support for the accuracy of our method and its applicability to detect novel signatures of interlocus gene conversion.

DISCUSSION

What would be required to obtain the same volume of genotype information for an arbitrary gene family comparable to *SRGAP2* or *RH* using existing approaches? WGS offers great potential given its comprehensive nature[1,25], but it remains prohibitively expensive for genotyping projects of even moderate size, especially given that accuracy demands high coverage. More scalable available targeted methods, on the other hand, provide limited genotyping power. PCR-based strategies for copy-number genotyping query at most a few sites per reaction because PCR multiplexes poorly[40,41]. MLPA and MAPH allow for the simultaneous analysis of up to 50 loci, but even this greater scale of multiplexing cannot match the ability of our method to assay many gene families each at high spatial resolution. None of the targeted methods above provides exonic sequence information, and none has been successfully applied in large-scale studies of gene conversion. As our analyses demonstrate, genetic variation in duplicated genes exhibits considerable complexity. Any method for genotyping such genes should be developed with this consideration in mind.

Although we focused on *SRGAP2* and *RH*, our method will be useful for studying other duplicated genes that have proven difficult to genotype accurately, including *CCL3L1* (refs. 19,20), beta-defensins[42,43] and *C4* (ref. 44) (Online Methods). We provide programs to obtain genotypes with confidence scores from MIP-sequence data and to assist in the identification of informative sites from aligned sequences (https://github.com/xnuttle/mips_cnv_typer/). We also provide a complete list of ~3.8 million SUNs based on the current human reference genome (GRCb37) for use with other duplicated regions and gene families (Online Methods and http://eichlerlab.gs.washington.edu/mips_cnv_typer/). Although higher copy number and more polymorphic gene families will pose additional challenges, generating high-coverage sequence data precisely over the most informative sites promises to significantly improve our understanding of genetic variation of these complex regions of the genome.

Successful application of our method to a particular gene family of interest depends on several factors, including availability of accurate sequence, the number of paralogs, their sequence identity, their GC content[31,32], their copy-number ranges and their sizes. First, optimal MIP design requires high-quality reference sequences for all family members, so gene families lacking complete sequence characterization (Online Methods and **Supplementary Table 8**) will be at least partially inaccessible using MIP-based genotyping. Second, some genetic variation must distinguish different paralogs from one another—our

method cannot determine copy number when copies are identical at the genomic level (<1% of all paralogous sequences). Third, gene families with high numbers of paralogs, or with paralogs at high copy numbers showing a range of copy-number variation, pose several challenges for MIP-based genotyping. In general, as the number of distinct paralogs increases, fewer potential target regions will contain SUNs allowing discrimination of all paralogs; thus, more MIPs will need to be designed for copy-number genotyping. Furthermore, paralog-specific read-count frequencies become more difficult to confidently distinguish as the aggregate copy number for a gene family increases. This particular issue could be mitigated somewhat via the use of single-molecule MIPs to quantify individual capture events[45]. Accurate sequence genotyping also becomes more difficult as the aggregate copy number increases and the number of possible assignments of sequences to paralog copies grows.

Our method will facilitate efforts to map NAHR-associated structural variation breakpoints, which often occur in complex regions of segmental duplication. Identifying SUNs that discriminate the high-identity paralogs followed by MIP genotyping will provide sequence-level precision to determine the effect of such rearrangements on the genes embedded in such complex regions[46]. We anticipate MIP-based genotyping will also be very valuable for studies of interlocus gene conversion, providing an experimental platform for surveying the most highly identical paralogs where this mechanism frequently operates[47]. In this study, we provide evidence of conversion-like events between paralogs separated by more than 80 Mbp—a somewhat surprising finding given that conversion is thought to occur most frequently between high-identity segments in close proximity[48–50]. Most notably, our MIP-based method will encourage the inclusion of many previously intractable duplicated genes in future genetic analyses of human phenotypes. With accurate, scalable genotyping, we will be well positioned to assess the impacts of hundreds of these genes on human traits and disease.

Associated software, documentation and an example data set are freely available via GitHub at https://github.com/xnuttle/mips_cnv_typer/.

METHODS

Methods and any associated references are available in the online version of the paper.

Accession codes. US National Center for Biotechnology Information Sequence Read Archive: SRP027257.

Note: Any Supplementary Information and Source Data files are available in the online version of the paper.

ACKNOWLEDGMENTS

We thank J. Kitzman for early ideas and enthusiasm for the project; P. Sudmant, E. Karakoc, F. Hormozdiari, B. Dumont and O. Penn for thoughtful discussion; L. Vives, K. Mohajeri and C. Lee for technical assistance; and T. Brown for assistance with manuscript preparation. X.N. is supported by a US National Science Foundation Graduate Research Fellowship under grant no. DGE-1256082. This work was supported by US National Institutes of Health grants HG004120 and HG002385 to E.E.E. E.E.E. is supported by the Howard Hughes Medical Institute.

AUTHOR CONTRIBUTIONS

X.N., J.S. and E.E.E. designed the study. X.N. and B.J.O. designed the MIPs. X.N. performed capture experiments, wrote analysis software and analyzed data. F.A. performed FISH experiments. J.H. contributed to the analysis software, prepared it for public access and identified SUNs from the reference genome. M.F. and C.R. contributed to sample collection. X.N. and E.E.E. wrote the paper, with input and approval from all coauthors.

COMPETING FINANCIAL INTERESTS

The authors declare competing financial interests: details are available in the online version of the paper.

1. Sudmant, P.H. *et al.* Diversity of human copy number variation and multicopy genes. *Science* **330**, 641–646 (2010).
2. Campbell, C.D. *et al.* Population-genetic properties of differentiated human copy number polymorphisms. *Am. J. Hum. Genet.* **88**, 317–332 (2011).
3. Redon, R. *et al.* Global variation in copy number in the human genome. *Nature* **444**, 444–454 (2006).
4. Sebat, J. *et al.* Large-scale copy number polymorphism in the human genome. *Science* **305**, 525–528 (2004).
5. Ohno, S. *Evolution by Gene Duplication* (Springer, New York, 1970).
6. Semple, C.A., Rolfe, M. & Dorin, J.R. Duplication and selection in the evolution of primate beta-defensin genes. *Genome Biol.* **4**, R31 (2003).
7. Han, M.V., Demuth, J.P., McGrath, C.L., Casola, C. & Hahn, M.W. Adaptive evolution of young gene duplicates in mammals. *Genome Res.* **19**, 859–867 (2009).
8. Bailey, J.A. & Eichler, E.E. Primate segmental duplications: crucibles of evolution, diversity and disease. *Nat. Rev. Genet.* **7**, 552–564 (2006).
9. Lefebvre, S. *et al.* Identification and characterization of a spinal muscular atrophy-determining gene. *Cell* **80**, 155–165 (1995).
10. Olbrich, H. *et al.* Recessive *HYDIN* mutations cause primary ciliary dyskinesia without randomization of left-right body asymmetry. *Am. J. Hum. Genet.* **91**, 672–684 (2012).
11. Bunge, S. *et al.* Homologous nonallelic recombinations between the iduronate-sulfatase gene and pseudogene cause various intragenic deletions and inversions in patients with mucopolysaccharidosis type II. *Eur. J. Hum. Genet.* **6**, 492–500 (1998).
12. Lupski, J.R. Genomic disorders: structural features of the genome can lead to DNA rearrangements and human disease traits. *Trends Genet.* **14**, 417–422 (1998).
13. Dennis, M.Y. *et al.* Evolution of human-specific neural *SRGAP2* genes by incomplete segmental duplication. *Cell* **149**, 912–922 (2012).
14. Doggett, N.A. *et al.* A 360-kb interchromosomal duplication of the human *HYDIN* locus. *Genomics* **88**, 762–771 (2006).
15. Locke, D.P. *et al.* Linkage disequilibrium and heritability of copy number polymorphisms within duplicated regions of the human genome. *Am. J. Hum. Genet.* **79**, 275–290 (2006).
16. McCarroll, S.A. & Altshuler, D.M. Copy-number variation and association studies of human disease. *Nat. Genet.* **39**, S37–S42 (2007).
17. Eichler, E.E. *et al.* Missing heritability and strategies for finding the underlying causes of complex disease. *Nat. Rev. Genet.* **11**, 446–450 (2010).
18. Manolio, T.A. *et al.* Finding the missing heritability of complex diseases. *Nature* **461**, 747–753 (2009).
19. Gonzalez, E. *et al.* The influence of *CCL3L1* gene-containing segmental duplications on HIV-1/AIDS susceptibility. *Science* **307**, 1434–1440 (2005).
20. Bhattacharya, T. *et al.* *CCL3L1* and HIV/AIDS susceptibility. *Nat. Med.* **15**, 1112–1115 (2009).
21. Cantsilieris, S., Baird, P.N. & White, S.J. Molecular methods for genotyping complex copy number polymorphisms. *Genomics* **101**, 86–93 (2013).
22. Armour, J.A.L. *et al.* Accurate, high-throughput typing of copy number variation using paralogue ratios from dispersed repeats. *Nucleic Acids Res.* **35**, e19 (2007).
23. Schouten, J.P. *et al.* Relative quantification of 40 nucleic acid sequences by multiplex ligation-dependent probe amplification. *Nucleic Acids Res.* **30**, e57 (2002).
24. Armour, J.A., Sismani, C., Patsalis, P.C. & Cross, G. Measurement of locus copy number by hybridisation with amplifiable probes. *Nucleic Acids Res.* **28**, 605–609 (2000).
25. Waszak, S.M. *et al.* Systematic inference of copy number genotypes from personal genome sequencing data reveals extensive olfactory receptor gene content diversity. *PLoS Comput. Biol.* **6**, e1000988 (2010).
26. Hardenbol, P. *et al.* Multiplexed genotyping with sequence-tagged molecular inversion probes. *Nat. Biotechnol.* **21**, 673–678 (2003).
27. Hardenbol, P. *et al.* Highly multiplexed molecular inversion probe genotyping: over 10,000 targeted SNPs genotyped in a single tube assay. *Genome Res.* **15**, 269–275 (2005).

28. Porreca, G.J. *et al.* Multiplex amplification of large sets of human exons. *Nat. Methods* **4**, 931–936 (2007).
29. Turner, E.H. *et al.* Massively parallel exon capture and library-free resequencing across 16 genomes. *Nat. Methods* **6**, 315–316 (2009).
30. Colin, Y. *et al.* Genetic basis of the RhD-positive and RhD-negative blood group polymorphism as determined by Southern analysis. *Blood* **78**, 2747–2752 (1991).
31. Wagner, F.F. & Flegel, W.A. *RHD* gene deletion occurred in the *Rhesus box*. *Blood* **95**, 3662–3668 (2000).
32. Kitano, T. & Saitou, N. Evolution of Rh blood group genes have experienced gene conversions and positive selection. *J. Mol. Evol.* **49**, 615–626 (1999).
33. O'Roak, B.J. *et al.* Multiplex targeted sequencing identifies recurrently mutated genes in autism spectrum disorders. *Science* **338**, 1619–1622 (2012).
34. Kidd, J.M. *et al.* Mapping and sequencing of structural variation from eight human genomes. *Nature* **453**, 56–64 (2008).
35. Bentley, D.R. *et al.* Accurate whole human genome sequencing using reversible terminator chemistry. *Nature* **456**, 53–59 (2008).
36. Lee, J.A., Carvalho, C.M. & Lupski, J.R.A. DNA replication mechanism for generating nonrecurrent rearrangements associated with genomic disorders. *Cell* **131**, 1235–1247 (2007).
37. Zhang, F. *et al.* The DNA replication FoSTeS/MMBIR mechanism can generate genomic, genic and exonic complex rearrangements in humans. *Nat. Genet.* **41**, 849–853 (2009).
38. Fledel-Alon, A. *et al.* Broad-scale recombination patterns underlying proper disjunction in humans. *PLoS Genet.* **5**, e1000658 (2009).
39. Carritt, B., Kemp, T.J. & Poulter, M. Evolution of the human RH (rhesus) blood group genes: a 50 year old prediction (partially) fulfilled. *Hum. Mol. Genet.* **6**, 843–850 (1997).
40. Edwards, M.C. & Gibbs, R.A. Multiplex PCR: advantages, development, and applications. *PCR Methods Appl.* **3**, S65–S75 (1994).
41. Markoulatos, P., Siafakas, N. & Moncany, M. Multiplex polymerase chain reaction: a practical approach. *J. Clin. Lab. Anal.* **16**, 47–51 (2002).
42. Groth, M. *et al.* High-resolution mapping of the 8p23.1 beta-defensin cluster reveals strictly concordant copy number variation of all genes. *Hum. Mutat.* **29**, 1247–1254 (2008).
43. Aldhous, M.C. *et al.* Measurement methods and accuracy in copy number variation: failure to replicate associations of beta-defensin copy number with Crohn's disease. *Hum. Mol. Genet.* **19**, 4930–4938 (2010).
44. Fernando, M.M. *et al.* Assessment of complement *C4* gene copy number using the paralog ratio test. *Hum. Mutat.* **31**, 866–874 (2010).
45. Hiatt, J.B. *et al.* Single molecule molecular inversion probes for targeted, high accuracy detection of low frequency variation. *Genome Res.* **23**, 843–854 (2013).
46. Itsara, A. *et al.* Resolving the breakpoints of the 17q21.31 microdeletion syndrome with next-generation sequencing. *Am. J. Hum. Genet.* **90**, 599–613 (2012).
47. Jackson, M.S. *et al.* Evidence for widespread reticulate evolution within human duplicons. *Am. J. Hum. Genet.* **77**, 824–840 (2005).
48. Schildkraut, E., Miller, C.A. & Nickoloff, J.A. Gene conversion and deletion frequencies during double-strand break repair in human cells are controlled by the distance between direct repeats. *Nucleic Acids Res.* **33**, 1574–1580 (2005).
49. Ezawa, K., Oota, S. & Saitou, N. Proceedings of the SMBE Tri-National Young Investigators' Workshop 2005. Genome-wide search of gene conversions in duplicated genes of mouse and rat. *Mol. Biol. Evol.* **23**, 927–940 (2006).
50. Chen, J.M. *et al.* Gene conversion: mechanisms, evolution and human disease. *Nat. Rev. Genet.* **8**, 762–775 (2007).

ONLINE METHODS

MIP design. *SRGAP2* exon-targeting MIPs were designed as previously described[33]. MIPs used for paralog-specific copy-number inference were designed in a similar fashion, with the following additional considerations. Careful selection of paralogous regions to target for MIP capture is critical for applying our copy-number genotyping method to any particular gene family of interest. Suitable target regions contain genetic variation between paralogs that has fixed in the human species. Obtaining paralog-specific read counts from a targeted region requires that the region contain genetic variation such that at least one paralog can be distinguished from all others. Ensuring that these counts reflect underlying relative paralog-specific copy numbers demands that variants used for distinguishing paralogs have very low levels of polymorphism.

To identify regions containing paralog-distinguishing variation, we aligned *SRGAP2* sequences[13], *RH* sequences (GRCb37/hg19, chr1:25594516–25655519 and chr1:25688914–25751819) and *RHD* flanking segmental duplications (GRCb37/hg19, chr1:25585374–25594516 and chr1:25655517–25664845) using Clustal 2.1 (ref. 51). Regions of the alignments where sequences identical between all paralogs (20 bp each side) flanked a 112-bp region where at least a single paralog had a distinct sequence were selected as potential targets and input to the MIP design pipeline[33]. This pipeline attempted to design MIPs to capture each of these potential target regions, outputting MIP oligonucleotides, information about their corresponding arm hybridization sequences and their capture targets, and scores corresponding to their predicted capture performances. We eliminated from consideration any MIPs determined to have arm hybridization sequences with copy counts in the genome (GRCb37 augmented with *SRGAP2* contig sequences) >8 to avoid capturing repeat sequences and to restrict MIP hybridization to *SRGAP2* and *RH* loci. We also ensured that all MIP arm hybridization sequences were complementary to sequences identical between all paralogs of interest—any MIPs not meeting this criterion were eliminated from further consideration. Finally, we eliminated from consideration all MIPs with the lowest design score (–1) and most MIPs having a target region with <35% or >55% GC content.

For remaining MIPs under consideration for design, we analyzed polymorphism at potential SUNs within the corresponding capture target regions. Briefly, potential SUNs distinguishing each paralog were extracted from the alignment and scored with regard to likely fixation status via analysis of 12 high-coverage genomes (**Supplementary Table 1**). For each *SRGAP2* and *RH* paralog, we computed all 30-mer sequences found within that paralog and absent from the rest of the genome (singly unique nucleotide *k*-mers[1] (SUNKs)). We then mapped 12 unrelated high-coverage genomes to *SRGAP2* and *RH* paralog sequences (masked using RepeatMasker[52] and Tandem Repeats Finder[53]) using mrsFAST[54] and parsed mapping output to assess the presence of each SUNK in each genome analyzed. A SUNK was considered present if observed in at least a single read mapped with no mismatches. Using only high-coverage genomes for this analysis minimizes the possibility of simply not having sequenced SUNKs that are truly present in a genome. Because each potential SUN typically contributes to (as a single base in the sequence of) many 30-mer SUNKs, the presence or absence of such SUNKs can serve as a proxy for the presence or absence of each potential SUN. Thus, a score from 0 to 12 was calculated for each potential SUN, corresponding to the average number of high-coverage genomes supporting a potential SUN's presence (**Supplementary Fig. 8**). For example, if a particular potential SUN contributed to four different 30-mer SUNKs, and these SUNKs were determined to be present in 11, 9, 11, and 12 high-coverage genomes, respectively, the score for that potential SUN would be 10.75 ((11 + 9 + 11 + 12)/4). True SUNs are paralog-distinguishing SNVs that have fixed in the human population. We defined potential SUNs having scores ≥11 (for *SRGAP2A*, *SRGAP2B*, and *SRGAP2C*) or ≥8 (for *SRGAP2D*, *RHD*, and *RHCE*) as true SUNs. (The threshold is lower for these latter paralogs owing to a paucity of higher-scoring potential SUNs across the spatial extent of duplicated sequence, reflecting in part heterozygous *SRGAP2D* and *RHD* deletions in some of the individuals sequenced to high coverage.) Biologically, these defined true SUNs are most likely to be fixed in a particular paralog in the human species and thus most useful for copy-number genotyping. Given the observation that the majority (84.8%) of putative autosomal SUNs genome-wide were present in 12 of 12 high-coverage genomes previously analyzed[1], however, SUN scoring, though useful, is not necessary for successful application of our method.

MIPs used for copy-number genotyping were selected from remaining MIPs under consideration on the basis of the paralog-specificity, SUN content, and relative genic location of their corresponding target regions. *SRGAP2A* and *SRGAP2C* were prioritized in the *SRGAP2* copy-number genotyping MIP design owing to the likely pseudogenicity of *SRGAP2B* and *SRGAP2D*[13]. All MIPs were ordered from Integrated DNA Technologies as previously described[33]. **Supplementary Table 2** provides specific details regarding MIPs designed for this study and their pooling.

MIP pooling, 5′ phosphorylation, and multiplex capture. MIPs were pooled (**Supplementary Table 2**), phosphorylated, and used to capture targeted sequences as previously described[33], with the following modifications. Initial capture reactions used in the 48-individual experiment were performed with genomic DNA input levels of 50 ng and 100 ng, with subsequent reactions involving HapMap samples using 200 ng DNA input and the reaction involving sample Troina2665 using 100 ng DNA input. MIPs were added to capture reactions at a ratio of 800 MIP copies per haploid genome copy. Incubation of capture reactions at 60 °C was performed for 23–24 h, and incubation of exonuclease reactions at 37 °C was performed for 45 min. **Supplementary Table 9** summarizes MIP capture experiments performed for this study and details sample sets assayed.

Amplification, barcoding, pooling, cleanup, and sequencing. Captured sequences were amplified, barcoded, pooled, and purified as previously described[33], with the following specifications. PCR was performed in a 25-µL reaction. Libraries with excessive off-target captures were not observed; thus, the standard Agencourt purification protocol was followed. Final library DNA concentrations were quantified using the Qubit dsDNA HS assay (Life Technologies). Sequencing of pools of capture reactions was performed using either a MiSeq or a HiSeq 2000, depending on the number of individual capture reactions included in the pool for sequencing and the number of MIPs used in each individual capture reaction. **Supplementary Table 9** provides specific

doi:10.1038/nmeth.2572

details regarding sequencing performed for different MIP capture experiments in this study.

Paralog-specific copy-number genotyping. Initial 151-bp reads (MiSeq) or 101-bp reads (HiSeq 2000) were trimmed from their 3′ ends to 76 bp to eliminate low-quality data from the ends of reads while ensuring coverage of each targeted base in nearly all cases. All MIPs are designed such that a 152-bp region (target sequence plus hybridization arms) is sequenced. With 151-bp reads, all bases except the first and last base in this 152-bp region are sequenced during both the forward and reverse reads. Thus, retaining only the first 76 bp from each read eliminates low-quality data from the ends of reads while ensuring coverage of each targeted base in all cases except those in which there is a net insertion. Trimmed reads were mapped to *SRGAP2* and *RH* paralog sequences using mrFAST 2.5 (ref. 55) in paired-end mode with the maximum allowed edit distance set to 4 and the minimum and maximum inferred distances allowed between paired-end sequences set to 144 and 160, respectively.

Mapping output was parsed to yield counts of reads mapping to each paralog for each MIP for each individual. The following stringent filters were applied to ensure accuracy: the mapping location of a read pair was required to be within 4 bp of the expected mapping location, the strandedness of reads had to be consistent with expectation based on MIP design, the inferred insert size had to be within 2 bp of its expected value (152 bp), any bases covered by forward and reverse trimmed reads had to have the same base call, the quality scores at all base positions showing variation between paralogs (base positions that affect mapping paralog-specificity) had to be at least Q30, no mismatches could occur at likely fixed true SUN positions, and reported barcode sequences had to perfectly match a known barcode sequence. Read pairs violating any of these filters were not included in final counts. For *SRGAP2* paralog-specific copy-number analysis, final counts served as input to a genotyping program that generated *SRGAP2* paralog-specific copy-number calls for each individual across the spatial extent of duplicated *SRGAP2* sequences. For *RH* paralog-specific copy-number analysis, genotyping calls were made in a similar automated fashion, except no copy-number state transitions were allowed. Thus, all internal *RH* gene conversion events were called on the basis of manual visual inspection of paralog-specific count frequency plots.

The *SRGAP2* genotyping program generates paralog-specific copy-number calls using a maximum-likelihood approach together with dynamic programming. For each individual, log-likelihoods of observing the paralog-specific read-count data for each MIP are calculated under 400 different possible hidden underlying *SRGAP2* paralog-specific copy-number states, where *SRGAP2A* and *SRGAP2C* can have copy numbers from 0 to 3 and *SRGAP2B* and *SRGAP2D* can have copy numbers from 0 to 4 ($4 \times 5 \times 4 \times 5 = 400$ combinations)[13]. For each paralog-specific copy-number state, log-likelihoods were calculated as logarithms of multinomial probabilities. Specifically, for each paralog-specific copy-number state, a multinomial probability of the observed data was computed for each MIP, with the number of trials equal to the total number of mapped reads for that MIP, and the vector of outcome probabilities equal to the copy numbers of specific paralogs over the aggregate copy number for the gene family given the paralog-specific copy-number state. (An outcome in this case is observing a read coming from a particular paralog.) The *SRGAP2D* internal deletion is built into the log-likelihood calculations: all copy-number states for MIPs in this region have *SRGAP2D* copy number set to 0. Log-likelihood values below −30 are set to −30 to limit the ability of count data from a single MIP to potentially single-handedly invalidate a particular *SRGAP2* paralog-specific copy-number state as possibly underlying the count data.

Next, for each individual, log-likelihoods are used to construct a weighted directed acyclic graph, with prior probabilities based on observed *SRGAP2* copy-number genotype data from previous experiments[13] incorporated into the log-likelihoods for the first (most 5′ with respect to *SRGAP2*) MIP. The graph is constructed by iteratively considering log-likelihoods for the next MIP and tracking the highest scoring paths ending at each copy-number state allowing 0, 1, and 2 transitions between copy-number states as well as the values of the corresponding log-likelihoods of these paths until the graph spans all MIPs. Allowed transitions between copy-number states are restricted to copy-number gains or losses affecting a single paralog or cases where the copy numbers of two paralogs change, but the total number of *SRGAP2* copies remains constant. All transitions meeting these criteria and transition probabilities associated with remaining in the same state have probability 1; all other transitions have probability 0. Three highest-scoring paths through the likelihood graph are calculated: one for 0 allowed total transitions between copy-number states, one for 1 allowed transition between copy-number states, and one for 2 allowed transitions between copy-number states. Restricting the nature of allowed copy-number state transitions reflects the fact that true biological events should fall into one of two categories (single paralog–affecting duplication/deletion or interlocus gene conversion). Restricting the number of transitions reflects the fact that a single individual is most likely to have, at most, a single duplication, deletion, or interlocus gene conversion restricted to within *SRGAP2*. If an individual were to have multiple events restricted to within *SRGAP2*, the program would still flag this individual as having a complex *SRGAP2* paralog-specific copy-number genotype, and the second internal event would be apparent upon subsequent visual inspection of paralog-specific count frequency plots. The program ultimately identifies the highest-scoring paths through the likelihood graph (most likely paralog-specific copy-number states across the spatial extent of duplicated *SRGAP2* sequence) allowing 0, 1, and 2 transitions and their corresponding log-likelihood scores. Heuristics (**Supplementary Table 10**) are used to assess increases in likelihood of the one-transition and two-transition paths compared to the zero-transition path and to determine whether they signal an event within *SRGAP2* and warrant calling the paralog-specific copy-number genotype for an individual as complex. In most cases, the scores of the one-transition and two-transition paths will not be substantially higher than that of the zero-transition path, and the genotype for an individual will be called as simple (a single copy-number state across the entirety of duplicated *SRGAP2* sequence).

The program also calculates a logarithm of odds confidence score associated with the simple (zero-transition) genotype call for each individual. Specifically, this score is equal to the log-likelihood of the chosen zero-transition path minus the highest log-likelihood for a zero-transition path having a distinct set of associated multinomial probabilities. For example, if an individual

was called as having two copies of each *SRGAP2* paralog, the confidence score would be the log-likelihood of the zero-transition path for this copy-number state minus the highest log-likelihood of a zero-transition path among all other copy-number states except those having equal copy numbers for each *SRGAP2* paralog. The logic behind this requirement is that likelihoods of zero-transition paths with the same set of associated multinomial probabilities will differ only because they have distinct prior probabilities—that is, the paralog-specific read-count frequency data, independent of any prior knowledge, support each such path equally well. Confidence scores should be interpreted relative to confidence scores for other individuals genotyped for the same gene family using the same set of MIPs (**Supplementary Table 7** and **Supplementary Fig. 5**) rather than in an absolute sense.

The *RH* genotyping program works the same way as the *SRGAP2* genotyping program, except that there are 25 different possible *RH* paralog-specific copy-number states (each of *RHD* and *RHCE* is allowed to vary in copy number from 0 to 4), prior probabilities used were based on our estimates of *RH* paralog-specific copy number from the 1000 Genomes Project (1KG) data, and no transitions between copy-number states were allowed, such that all *RH* genotypes are called as simple (a single copy-number state across the entirety of duplicated *RH* sequence).

Fluorescence *in situ* hybridization. Metaphase spreads were obtained from lymphoblast and fibroblast cell lines from human HapMap individuals NA19700, NA19703, NA19901, NA20127, NA20334, NA19005, NA19190, NA19201, and NA12878 (Coriell Cell Repository). FISH experiments were performed using fosmid clones (WIBR2-2926C23_G248P88292B12 and WIBR2-3738J10_G248P802587E5)[13] directly labeled by nick translation with Cy3-dUTP (Perkin-Elmer), Cy5-dUTP (Perkin-Elmer), and fluorescein-dUTP (Enzo) as described previously[56] with minor modifications. Briefly: 300 ng of labeled probe were used for the FISH experiments; hybridization was performed at 37 °C in 2× SSC, 50% (v/v) formamide, 10% (w/v) dextran sulfate, and 3 μg sonicated salmon sperm DNA in a volume of 10 μL. Posthybridization washing was at 60 °C in 0.1× SSC (three times, high stringency). Nuclei were simultaneously DAPI stained. Digital images were obtained using a Leica DMRXA2 epifluorescence microscope equipped with a cooled CCD camera (Princeton Instruments). DAPI, Cy3, Cy5 and fluorescein fluorescence signals, detected with specific filters, were recorded separately as grayscale images. Pseudocoloring and merging of images were performed using Adobe Photoshop software.

Other orthogonal validations. Array CGH data, qPCR data, and whole-genome shotgun sequence data from the 1KG used for validation purposes were collected and processed as previously described[1,13].

Paralog-specific SNV genotyping. We trimmed initial reads from their 3′ ends to 100 bp to eliminate some low-quality data from the ends of reads while ensuring coverage of each targeted base. Trimmed reads were mapped separately to individual *SRGAP2* paralog sequences using the Burrows-Wheeler Aligner[57] (v.0.5.9, paired-end mapping) with the following options: -e 50 -l 17 -q 20 -d 5 -i 5 -I. Mapping output, combined with each individual's *SRGAP2* paralog-specific copy-number genotype determined as described above, was parsed to yield sequence genotypes for each copy of each paralog for each MIP for each individual. The Hungarian method[58] was used to optimally assign distinct sequences to copies of different *SRGAP2* paralogs according to observed counts of distinct sequences, treating paralog-specific mapping edit distances as the costs of sequence assignments to copies of different paralogs. In cases where equally optimal but biologically distinct sets of assignments could be made, each assignment set and its corresponding paralog-specific sequence genotypes was reported and flagged as having some ambiguity. All detected SNVs were annotated with regard to location and likely functional impact. Reported SNVs in **Supplementary Table 6** have the following properties: (i) they were called on the basis of MIP sequence data from NA18507, (ii) they occur at alignment positions where all paralogs share the same nucleotide, (iii) they occur in close proximity to a SUN or on a paralog-distinguishing haplotype such that their paralog-of origin can be accurately inferred, (iv) they were unambiguously assigned to a particular paralog, and (v) all copies of the paralog they were assigned to have no ambiguity in sequence at the variant site.

Preparation of final *SRGAP2* MIP pool. Data from the 48-individual genotyping experiment revealed that most MIPs in the initial pool captured their corresponding targets well (**Supplementary Fig. 9**). Considering only the capture reactions using 100-ng DNA input, the mean and median mapped read counts per MIP were 18,447 and 15,809, respectively. On average, this translates to approximately 350 mapped reads per MIP per individual. To optimize our MIP pool before extending our genotyping efforts to thousands of samples, we rebalanced exon-targeting MIPs that failed to efficiently capture their corresponding targets and removed *SRGAP2* copy-number genotyping MIPs that did not meet a high performance standard.

Specifically, we increased the amount of any exon-targeting MIPs having a total mapped read count lower than 2,500 times the number of paralogs that include the targeted exon. For example, if a MIP targeted exon 1, shared between all four *SRGAP2* paralogs, but had fewer than 10,000 reads from the initial capture reactions using 100-ng DNA input, we rebalanced it. Rebalancing was performed such that this count threshold would be achieved if mapped read count per MIP increases proportionally with the amount of MIP added to the pool: for example, if doubling the amount of MIP added to the pool results in twice the number of corresponding mapped reads. We thus added seven exon-targeting MIPs to achieve a relative amount of 2× in the final pool and another five such MIPs to achieve a relative amount of 5×. Eleven MIPs, however, would still fail to meet the count threshold even if their corresponding mapped read counts increased fivefold. These worst-performing exonic MIPs were added to achieve a relative amount of 50× in the final MIP pool to maximize their chances for successful capture.

To evaluate the performance of *SRGAP2* copy-number genotyping MIPs, we compared observed paralog-specific count frequencies for each MIP with corresponding expected frequencies for 31 genomes from the 48-individual experiment (**Supplementary Table 3**). These genomes were selected because we had very high confidence in their true paralog-specific copy-number genotypes: genotyping results were concordant between all methods used for 30 of these genomes, and FISH results supported MIP results

doi:10.1038/nmeth.2572

in the remaining case. For each *SRGAP2* copy-number genotyping MIP, we calculated the mean and s.d. of per-genome error in paralog-specific count frequencies (**Supplementary Fig. 1**). We removed MIPs having mean per-genome errors ≥0.125 or corresponding s.d. ≥0.25 from our final set, with a few exceptions. For example, we retained some MIPs in the *SRGAP2C* deletion region having mean errors or s.d. slightly above these values because we wanted to maximize our power to genotype this event. Reducing the number of MIPs used for genotyping *SRGAP2* in our final pool in this manner increases our capacity to assay additional genes of interest and larger numbers of individuals in the same experiment while ensuring *SRGAP2* genotyping remains highly accurate. Selection of a high-performing final MIP set from all initial MIPs tested, though useful for increasing multiplexing potential, is not necessary for successful application of our method (**Supplementary Fig. 2**).

Cost estimation. The approximate cost per gene per individual associated with using MIPs can be estimated as follows. Each MIP is 70 bp, and each synthesized base costs $0.09. Thus, each MIP costs $6.30. We usually multiplex ~2,000 MIPs in a single MIP pool, so the cost of generating a typical MIP pool is $12,600. Because a very small amount of the MIP pool is used in each capture reaction, a single order of oligonucleotides can be used to assay tens of thousands of samples; thus, we assume this cost is effectively fixed (i.e., independent of the number of samples tested). The oligo cost per sample thus depends on the number of samples tested. Assuming we assay 4,000 samples, for example, the per-sample oligo cost is $3.15. The cost of reagents associated with the experimental protocol is $2.57 per sample. The cost of a lane of sequencing using the HiSeq is $1,388. We have found that up to 192 samples can be multiplexed per lane to obtain high coverage per MIP per sample under the assumption that the MIP pool used in capture experiments contained 2,000 MIPs. Thus, the sequencing cost per sample is approximately $7.23. Adding these results, we obtain a cost of $12.95 per sample. Assuming each gene can be effectively assayed by 50 MIPs, on average, each MIP pool covers 40 genes. Thus, the final cost per gene per sample in this scenario is ~$0.32. If we eventually assay 10,000 samples using this same MIP pool, the final cost per gene per sample works out to $0.28. Even if we were to assay only 1,000 samples, the final cost per gene per sample would still be less than $1 (~$0.56).

Internal deletion and duplication genotyping by WGS. We leveraged data from the 1KG to evaluate WGS-based discovery of novel structural variation within duplicated genes and to compare these results with our MIP data. Specifically, we genotyped *SRGAP2B* copy number in an individual genotyped by MIPs as having two copies of *SRGAP2B* with an 83-kbp internal *SRGAP2B* duplication, and we genotyped *SRGAP2C* copy number in seven individuals genotyped by MIPs as having two copies of *SRGAP2C*, one harboring the 38-kbp internal deletion. All WGS-based paralog-specific copy-number estimates[1] for these individuals were 2; however, specifying the regions affected by these events before genotyping allowed for successful identification of the internal events in 7 of 8 cases (**Supplementary Table 11**). These data provide additional support for the internal duplications and deletions called by our MIP-based method and suggest that naive paralog-specific copy-number genotyping using low-coverage WGS data cannot reliably discover them.

Application of our method to other gene families of interest. To use our method to study a gene family of interest other than *SRGAP2* or *RH*, one would first need to obtain accurate genomic sequences for as many paralogs as possible. Having reliable sequence data for all paralogs allows MIP design to be optimized to achieve complete paralog specificity and maximize genotyping power. Second, one would align paralogous sequences and identify SUN-containing regions to guide MIP design. We provide a program (https://github.com/xnuttle/mips_cnv_typer/) to identify such regions from aligned sequences. Third, one would attempt to design MIPs to all such regions as well as exons using the publicly available MIP design software[33], select a final set of MIPs according to criteria detailed above, and order them from a commercial oligo provider. Fourth, one would perform the MIP experiments and analyses described (https://github.com/xnuttle/mips_cnv_typer/) to obtain genotypes for each duplicated segment. If possible, we recommend testing every new MIP set on a panel of genomes having known paralog-specific copy numbers to ensure accuracy and reproducibility.

We found *RH* more difficult to genotype for copy number than *SRGAP2* using our approach. Two factors likely contribute to this observation. First, *RH* paralog-specific copy-number genotyping included data from only 35 MIPs, whereas that for *SRGAP2* incorporated data from either 90 or 142 MIPs. Second, fewer independent MIP capture events occur per genome for *RH* than *SRGAP2* because there are fewer total genomic copies of *RH* than *SRGAP2*. Thus, there are effectively fewer experimental trials for *RH* than *SRGAP2*, resulting in increased sampling error in *RH* paralog-specific read-count data. Designing more MIPs targeting *RH* and increasing DNA input would mitigate these issues and improve future *RH* genotyping performance. These issues warrant consideration in applying our method to other gene families of interest.

CCL3L1 (refs. 19,20,59,60), beta-defensins[42,43], and *C4* (ref. 44) present a few novel challenges for our method: (i) *CCL3L1* and beta-defensins are much smaller than *SRGAP2* and *RH*, such that only a few MIPs may be able to interrogate SUN-containing regions within them; (ii) unlike *SRGAP2* and *RH*, beta-defensins and *C4* have no obvious family member fixed or nearly fixed at diploid copy number 2 in the human population, making copy-number determination based on relative counts more ambiguous. For these gene families, it will be necessary to perform absolute in addition to relative read depth analysis, perhaps via singular value decomposition analysis as has been done to normalize exome capture variability from a large number of samples[61]. Another possible strategy would be to use some MIPs as MLPA probes (**Supplementary Fig. 10**) targeting genes of interest and regions of known invariant diploid copy number to calibrate aggregate or paralog-specific copy-number estimates on the basis of absolute read depth data. In addition, genotyping copy number of the blocks of duplicated sequence containing *CCL3L1* and beta-defensins should provide accurate copy-number genotypes for these genes, as common copy-number variation at these loci occurs at the level of such blocks rather than affecting individual genes within them[47]. This approach leverages the

much larger sample of SUNs these blocks contain compared to the genes themselves.

Identification of missing paralogous sequences in GRCb37. We genotyped regions in GRCb37 that had been previously described as missing paralogous sequence in GRCb36 (ref. 1) to identify regions of the reference genome still lacking complete sequence characterization. We successfully lifted over 326 of the original 333 regions from GRCb36 to GRCb37 and calculated paralog-specific copy numbers for each region with 885 individuals from the 1KG. A region was considered 'missing' from GRCb37 if the paralog-specific copy number for that region was greater than 2 for at least 90% of the individuals we genotyped. Using this definition, we found 21 regions that are still missing paralogous sequence in GRCb37. Comparing these regions with public NCBI patches to GRCb37 reveals that 7 of the 21 regions are completely covered by a fix patch and will likely be resolved in GRCb38.

Identification of SUNs from GRCb37. We used previously calculated SUNKs and segmental duplications for GRCb37 to calculate the set of all SUNs that uniquely identify individual segmental duplications. For each pair of segmental duplications, we globally aligned the corresponding sequences and identified all mismatches, insertions and deletions. We identified the diagnostic differences between related duplications by intersecting the coordinates of all differences with coordinates for SUNKs across GRCb37. With this approach we identified ~4 million SUNs. After filtering out any of these SUNs that were within 36 bp of repeats identified by RepeatMasker[52] or Tandem Repeats Finder[53], we identified ~3.8 million SUNs.

51. Thompson, J.D., Gibson, T.J. & Higgins, D.G. Multiple sequence alignment using ClustalW and ClustalX. *Curr. Protoc. Bioinformatics* **1**, 2.3 (2002).
52. Tarailo-Graovac, M. & Chen, N. Using RepeatMasker to identify repetitive elements in genomic sequences. *Curr. Protoc. Bioinformatics* **25**, 4.4 (2009).
53. Benson, G. Tandem repeats finder: a program to analyze DNA sequences. *Nucleic Acids Res.* **27**, 573–580 (1999).
54. Hach, F. *et al.* mrsFAST: a cache-oblivious algorithm for short-read mapping. *Nat. Methods* **7**, 576–577 (2010).
55. Alkan, C. *et al.* Personalized copy number and segmental duplication maps using next-generation sequencing. *Nat. Genet.* **41**, 1061–1067 (2009).
56. Antonacci, F. *et al.* A large and complex structural polymorphism at 16p12.1 underlies microdeletion disease risk. *Nat. Genet.* **42**, 745–750 (2010).
57. Li, H. & Durbin, R. Fast and accurate short read alignment with Burrows-Wheeler Transform. *Bioinformatics* **25**, 1754–1760 (2009).
58. Kuhn, H.W. The Hungarian Method for the assignment problem. *Nav. Res. Logist. Q.* **2**, 83–97 (1955).
59. Carpenter, D., Walker, S., Prescott, N., Schalkwijk, J. & Armour, J.A. Accuracy and differential bias in copy number measurement of *CCL3L1* in association studies with three auto-immune disorders. *BMC Genomics* **12**, 418 (2011).
60. Nordang, G.B. *et al.* Association analysis of the *CCL3L1* copy number locus by paralogue ratio test in Norwegian rheumatoid arthritis patients and healthy controls. *Genes Immun.* **13**, 579–582 (2012).
61. Krumm, N. *et al.* Copy number variation detection and genotyping from exome sequence data. *Genome Res.* **22**, 1525–1532 (2012).

doi:10.1038/nmeth.2572